

Anomalous temperature dependence of local magnetic fields in altermagnetic MnTe

Thomas J. Hicken,^{1,*} Oliver Amin,² Alfred Dal Din,² J. Hugo Dil,^{3,4} Dominik Krieger,⁵ Hubertus Luetkens,¹ Helena Reichlová,⁵ Zaher Salman,¹ Klára Uhlířová,⁶ Peter Wadley,² Juraj Krempaský,³ and Jonas A. Krieger^{1,†}

¹*PSI Center for Neutron and Muon Sciences, 5232 Villigen PSI, Switzerland*

²*School of Physics and Astronomy, University of Nottingham, Nottingham, United Kingdom*

³*Photon Science Division, Paul Scherrer Institut, Villigen, Switzerland*

⁴*Institut de Physique, École Polytechnique Fédérale de Lausanne, Lausanne, Switzerland*

⁵*Institute of Physics, Czech Academy of Sciences, Prague, Czech Republic*

⁶*Faculty of Mathematics and Physics, Charles University, Prague, Czech Republic*

Altermagnets are a novel type of magnetic system that has a spin-polarised electric band structure in the absence of a net magnetic moment, leading to exciting prospects in potential device applications. Hexagonal MnTe, a prototypical altermagnet, has arguably shown the most properties consistent with theoretical predictions, including an anomalous Hall effect despite no net magnetisation, and strong altermagnet-induced spin splitting in the electronic band structure. Here we present muon-spin spectroscopy measurements of a single crystal of MnTe. Below room temperature we observe pronounced anomalies in the muon-spin depolarisation, as well as the onset of a second, non-proportional internal field in the absence of an applied field. These findings point to a change in the magnetic structure around $T \simeq 250$ K, which coincides with other changes in reported properties, such as transport.

I. INTRODUCTION

Magnetically ordered solids are traditionally divided into two elementary phases: ferromagnets and antiferromagnets. A key characteristic of ferromagnets is a macroscopic magnetisation due to the local alignment of neighbouring magnetic moments, and this net magnetisation leads to a spin-polarised electronic structure and the anomalous Hall effect. On the other hand, collinear antiferromagnets lack a net magnetisation due to a compensated magnetic order, yielding a spin degenerate band structure. Recently, a third fundamental collinear magnetic phase, known as altermagnetism, was discovered [1], which combines aspects of both ferromagnetism and antiferromagnetism.

Altermagnetism is characterised by a compensated collinear magnetic order in real space, specifically opposite spin sublattices connected by crystal rotation symmetries (symmorphic/non-symmorphic, proper/improper). In reciprocal space, unconventional spin polarised bands with corresponding rotational symmetries manifest. This real-to-reciprocal-space correspondence results in electronic band structures with broken time reversal symmetry and alternating momentum dependent signs of spin splitting [2]. These properties, despite the compensated magnetic structure, result in new physical phenomenon, underpinning fundamental science and opening the possibility of realising robust spintronic memories, charge-spin conversion devices, and optospintronics [3].

Hexagonal MnTe has recently attracted significant attention as a prototypical altermagnet. Below its ordering

temperature of $T_c \simeq 310$ K, it consists of ferromagnetically ordered Mn layers, which are stacked such that magnetic moments in alternating layers point in the opposite direction [4–6]. Furthermore, the two spin sublattices are related by a six fold crystal rotation combined with a half-unit cell translation. Despite having no net magnetisation and collinear spin ordering, MnTe demonstrates an anomalous Hall effect [7], which cannot occur in conventional antiferromagnets. Furthermore, previous photoemission experiments have observed the giant band splitting that was predicted due to the altermagnetic lifting of the Kramer’s spin degeneracy [8]. Moreover, MnTe has specifically been suggested as a promising platform for magnetic memory applications [9].

Given these observations, detailed studies of the magnetism with various experimental probes is essential. To be able to use MnTe for device applications, microscopic control of the domains is needed [10]; thus a complete picture of the realised magnetic structure(s) is crucial. Further, this knowledge is required to fully understand other reported measurements of MnTe, such as the spin-split bandstructure and transport properties. In this paper, we employ muon-spin spectroscopy (μ SR), a local probe technique that is incredibly sensitive to the precise details of the magnetic structure. μ SR has previously been used to study other altermagnets such as $\text{Co}_{1/4}\text{NbSe}_2$ [11], where it confirmed the magnetic structure was consistent with that required for altermagnetism. Here we demonstrate, through careful μ SR measurements of a single crystal of MnTe, that the magnetic structure is more complicated than previously appreciated, with temperature-dependent changes in the realised configuration.

* thomas.hicken@psi.ch

† jonas.krieger@psi.ch

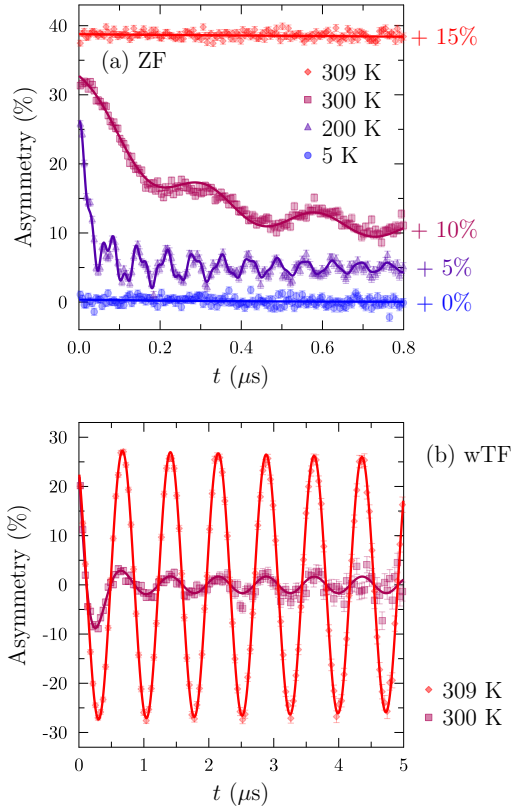


FIG. 1. **Fitted μ SR spectra of MnTe.** (a) Zero-field (ZF) measurements are sensitive to the internal field; coherent oscillations reveal long-range magnetic order below $T_c \simeq 308$ K, with a change in the magnetism around $T^* \simeq 250$ K. Spectra are offset for clarity. (b) Weak-transverse field measurements reveal the non-magnetic volume fraction of the sample, which is equal to the long-lived oscillating fraction. Above T_c there is no long-range magnetic order, whereas below T_c MnTe is fully ordered.

II. RESULTS

Our zero-field (ZF) μ SR measurements of single-crystal MnTe reveal three distinct temperature regions below T_c , each of which show a different magnetic response. In a ZF- μ SR experiment, 100% spin-polarised muons are implanted in the material, stopping at interstitial sites where they precess in the local internal field. After, on average, $2.2 \mu\text{s}$, the muon decays into two neutrinos and a positron, which is preferentially emitted in the direction the muon-spin was pointing at the time of decay. Hence, by detecting positrons from many muon implantations, we can track the time evolution of the muon-spin, and understand how the local magnetic field in the sample evolves.

Representative ZF μ SR spectra are shown in Fig. 1(a), with more details on the fitting procedure given in Sec. IV. Above T_c , which we find to be approximately 308 K in our measurements, we observe weak relax-

ation of the μ SR asymmetry (directly proportional to the muon-spin polarisation), typical of the dynamics of a paramagnet. We further confirm this observation by applying a small field (10 mT) perpendicular to the initial direction of the muon-spin. In these weak-transverse field (wTF) measurements only muons that stop in non-magnetic regions will precess in the applied field. As shown in Fig. 1(b), we obtain an oscillating asymmetry of $27.43(14)\%$, consistent with the maximum asymmetry on the instrument, thereby confirming there is no long-range magnetic order above T_c . Conversely, below T_c there are two components in the wTF asymmetry; a fast-relaxing component arising from muons stopping inside the sample that are predominantly sensitive to the internal field arising from long-range magnetic order, and a long-lived oscillating fraction attributed to muons stopping outside of MnTe (accounting for $6.1(5)\%$ of the total measured muons) and are hence sensitive to the applied field. It is therefore clear that the MnTe single crystal is fully magnetically long-range ordered.

Below $T_c \simeq 308$ K, but above $T^* \simeq 250$ K, our ZF μ SR reveals the first magnetically ordered regime. In this regime, the asymmetry spectra are well characterised by two components, a damped oscillation with amplitude A_{osc} and an average internal field B_1 in Fig. 2, corresponding to muons stopping in long-range magnetically ordered regions, and a strong relaxation at early times, A_{rel} , corresponding to muons subject to a large distribution of fields, with an average around zero, see Eqn. 2. This fast, early-time relaxation suggests that there is a significant fraction of the sample that is relatively disordered, such as in magnetic domain walls. Such domain walls, including vortex-like structures, have previously been observed in microscale MnTe structures [10]. As the temperature decreases, the relaxation rates of both of these components (Λ_{B1} and λ_{rel}), which are proportional to the width of the field distribution at the muon site, increase.

At $T^* \simeq 250$ K we reach a maximum in Λ_{B1} , as well as seeing the appearance of a second frequency in the spectra below T^* . Throughout this regime, the amplitude of this second oscillatory component is temperature-independent ($38.1(9)\%$ of the A_{osc}). This suggests a change in the magnetic structure sensed by the muon, and will be discussed further in Sec. III. In this phase, which extends down to at least $T \simeq 160$ K, the two internal fields [Fig. 2(a)] follow different scaling laws (i.e. they are not simply a fixed multiple of each other). This abnormal observation can be explained either by phase separation into two macroscopically distinct phases, or by a continual evolution of the magnetic structure over this temperature range. Given that the temperature independence of the ratio between the amplitudes of the two components, and that they are approximately equally weighted, it is most likely that the two components are indeed coming from the same, continually evolving magnetic order (i.e. there is no macroscopic phase separation). This is further evidenced by the kink in the tem-

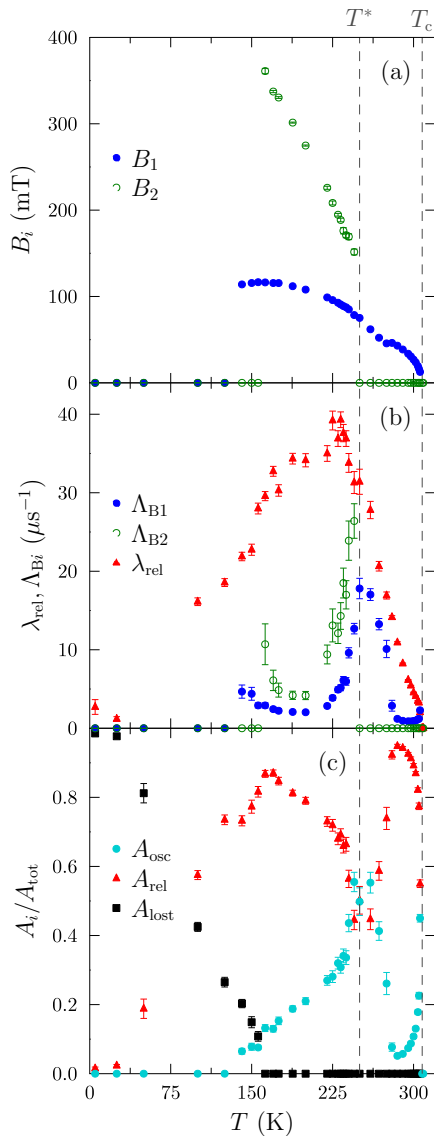


FIG. 2. **Fitted parameters from zero-field muon-spin spectroscopy measurements of single-crystal MnTe.** Each panel shows different extracted fitting parameters, as detailed in the main text. (a) The average internal field(s) B_i at the muon stopping site, reveals a change in magnetic behaviour around $T^* \simeq 250$ K. (b) The relaxation rates Λ_{B_i} and λ_{rel} are sensitive the width of the distribution of fields sensed by the muon, either centered around B_i , or zero (λ_{rel}). (c) The relative amplitude of each component A_i (normalised by the temperature independent total asymmetry A_{tot}), with A_{osc} representing the total oscillating fraction, and A_{lost} the amount of the spectra that relaxes too quickly to be observed.

perature evolution of B_1 , which would not be expected to occur in the case of magnetic phase separation. We note that the onset of this kink and the appearance of the second oscillation are not observed at the exact same temperatures for both frequencies. This is most likely due to the high damping rates around T^* which make the higher oscillation frequency more difficult to resolve

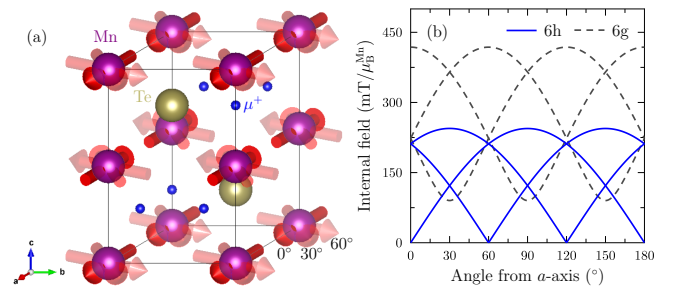


FIG. 3. **Muon site, considered magnetic structures, and corresponding dipole field calculations, for MnTe.** (a) To explain the temperature-dependent magnetic structure, we propose a rotation of the magnetic-easy axis within the $a-b$ plane, as shown in the figure. The occupied muon site, sitting at a 6h Wyckoff site, is indicated. (b) This muon site and magnetic structure is used to calculate the dipole field to which the muon is sensitive. Rotation of the easy-axis within the $a-b$ plane can explain the experimental μSR data.

in the spectra until the two internal fields are sufficiently different.

At lower temperatures we observe a reduction in the initial asymmetry (below $T \simeq 160$ K), and a disappearance of both oscillating components (with the high frequency component not resolvable below $T \simeq 160$ K, and the lower frequency also not resolvable below $T \simeq 125$ K). This indicates that the internal fields and/or relaxation rates become too high to resolve with μSR (i.e. the asymmetry dephases before we are able to measure it). One explanation of this could be that the disordered regions, seen at all T through the solely-relaxing A_{rel} component dominant the sample volume, perhaps due to an unusual decrease of correlation length towards low temperatures, or due to significant dynamics on the muon-timescale due to a dynamic process.

III. DISCUSSION

To understand our ZF μSR results better, we have performed muon stopping site calculations, finding two potential sites. In our calculations, muons clustered around the 6g ($1/2, 0, 0$) and 6h ($1/3, 1/6, 1/4$) Wyckoff positions, with the 6g approximately 0.2 eV lower in energy. In general, it is not currently possible to calculate the expected stopping fraction of muons in two crystallographically inequivalent sites [12] as it is a complex problem depending on the energy barrier to enter each site. We observe the 6g site disturbs the surrounding atoms more than the 6h site, possibly suggesting it is likely to have a larger barrier to occupation. To work out the stopping fraction in each site, we instead turn to magnetic dipole field calculations.

We have calculated the dipole field at the two candidate muon sites assuming the accepted magnetic structure of [4–6], that of two opposite spin sublattices. For

this structure it has been challenging to unambiguously determine the magnetic easy-axis for certain. We therefore take a cautious approach and simply consider, for the known two opposite spin sublattices with various in-plane oriented magnetic moments, how we can reproduce the μ SR spectra. With this constrain, we are unable to reproduce a single, finite field at the 6g muon site (finding instead that the crystallographically equivalent sites are magnetically inequivalent). Conversely, the 6h site accurately reproduces the experimental spectra at high T when the magnetic easy-axis lies along the crystallographic a -axis. We therefore conclude that the 6g site is unoccupied, and the muons stop at the 6h site. This site is shown, along with the magnetic structures, in Fig. 3.

Our calculations suggest that, at the occupied 6h site, there are three magnetically inequivalent sites. Two of these are accidentally degenerate when the easy-axis of the magnetic structure lies along the a -axis (0° in Fig. 3), with the magnetic field vector in our calculations giving the projection onto the different detectors that we expect from our experiment. At the third site, the dipole field cancels out, leading to a significant fraction of the muons that will be sensitive to close-to-zero dipole fields, accounting for at least a fraction of the solely-relaxing A_{rel} component seen experimentally. We note that more than one-third of muons correspond to the A_{rel} component, hence there is still a non-negligible fraction of domain-wall like, disordered regions, however the volume fraction of these is not as large as is perhaps initially thought.

To further understand the appearance of the second frequency, which we have already established signifies a change of the magnetic structure around $T^* \simeq 250$ K, we consider a rotation of the easy-axis of the magnetic structure within the $a - b$ plane, away from the a -axis. This rotation breaks the accidental degeneracy of the two magnetically inequivalent muon sites, and will result in an additional field appearing in the μ SR spectra. At 30° , we once again obtain accidental degeneracy of the two sites, however at this angle it results in two finite fields, consistent with our experimental data. This corresponds to the easy axis proposed in Ref. [6] for MnTe. To explain the temperature-dependent ratio between the two internal fields that we observe experimentally, we would need to allow another continuous change in the magnetic structure. A likely explanation would be an additional rotation or a canting of the magnetic moments that evolves as a function of temperature and which might lead to a weak net magnetisation, as suggested in Ref. [13]. We find that a number of other subtle changes to the magnetic structure can maintain the accidental degeneracy of two of the sites, whilst having a significant impact on the ratio between the two internal fields.

Whilst the observation of a second magnetic phase is perhaps surprising, there are a number of other techniques that have observed changes around $T \simeq 250$ K, supporting our observation. In micrometre sized structures of MnTe, Ref. [10] reports the existence of the anomalous Hall effect (AHE), and x-ray magnetic cir-

cular dichroism (XMCD) magnetic contrast at lower T (150 K and 100 K respectively), but both are absent at 250 K. Both the XMCD signal [10, 14] and the AHE [7, 15] are expected to strongly depend on the angle in $a - b$ plane of the altermagnetic order vector, and should vanish completely when the moments point along the a -direction, consistent with our observations. In other works [16, 17], there have been reports of significant changes in the angle-resolved photoemission spectroscopy around $T \simeq 250$ K. This transition has sometimes been taken as the paramagnetic transition, however may be better explained by a change in the long-range magnetic order.

One can also consider whether or not the change in magnetic easy-axis would be expected theoretically. Much density functional theory (DFT) work has been undertaken on MnTe, with one key result being that, despite the inclusion of a Hubbard U being essential for stabilisation of the correct magnetic structure [18], the inclusion of spin-orbit coupling makes much less difference [19]. Furthermore, in calculations of the magnetocrystalline anisotropy, the energy difference for different in-plane moment orientations was found to be very small [6], which is also experimentally supported by the fact that the magnetic moments can be rotated with a magnetic field [9]. It therefore seems very plausible, with only weak coupling between the magnetic moments and the lattice, that a temperature dependent magnetic easy axis may be realised.

IV. CONCLUSIONS

We have performed μ SR measurements of bulk MnTe, which reveals that the system possesses at least two distinct magnetic regimes, which can be explained by a change in the magnetic structure around $T^* \simeq 250$ K. Specifically, we suggest that below T^* , the magnetic easy-axis lies 30° from the a -axis, as has been previously considered. However, additional modifications to the magnetic structure that continuously evolve as a function of temperature may be needed to fully explain the μ SR spectra down to temperatures of at least ~ 100 K where the damping becomes too large for the details of the magnetic oscillations to be resolvable. At higher temperature, above T^* , the magnetic easy axis rotates, pointing along the a -axis. Further evidence for this change comes in the form of other experimental techniques, and is supported by theoretical calculations. Given the important role MnTe plays as the prototypical altermagnet [8], it is important to resolve these changes in the magnetic structure such that accurate theoretical predictions of different experimental measurements can be made. These discoveries were made possible due to the extreme sensitivity of μ SR to subtle changes in the magnetic structure, demonstrating the necessity of using the technique to explore other materials, such as altermagnets, where precise details of the magnetic structure are important.

ACKNOWLEDGMENTS

Part of this work was carried out at S μ S, Paul Scherrer Institute, Switzerland, and we are grateful for the provision of beamtime. Single-crystal were grown in MGML (mgml.eu), which is supported within the Program of Czech Research Infrastructures, grant no. LM2023065. We would like to thank G. Janka, T. Prokscha, G. Springholz, and A. Suter for fruitful discussions.

COMPETING INTEREST

The authors declare no competing interests.

DATA AVAILABILITY

The data of this study will be made available before publication.

EXPERIMENTAL AND COMPUTATIONAL DETAILS

μ SR measurements were performed using the GPS spectrometer [20] at S μ S, Paul Scherrer Institute, Switzerland. A large single crystal was used such that the a -axis was oriented along the muon-momentum direction (along the forward-backward detectors), with the muon spin rotated 60° towards the c -axis (aligned along the up-down detectors). With this geometry, measurements are simultaneously sensitive to two components of the internal field.

Our wTF μ SR measurements were fitted by

$$A_{\text{wTF}} = \sum_{i=1}^2 A_i \exp(-\Lambda_i t) \cos(\gamma_\mu B t + \phi), \quad (1)$$

where the two components with amplitudes A_i correspond to muons that stop in different locations; magnetically ordered regions, and magnetically disordered regions. Above T_c only one component is needed, as the sample is magnetically disordered. The fitted $B \simeq 10$ mT, very close to the applied field as expected, and $\phi \simeq 30^\circ$ or 60° for the Up-Down and Forward-Backward detectors respectively, confirming the

spin rotation. The relaxation rate Λ_i reflects a distribution of fields at the muon site, and is large ($\simeq 5 \mu\text{s}^{-1}$) when sensitive to long-range order in MnTe, and small ($\simeq 0.01 \mu\text{s}^{-1}$) for muons that stop outside MnTe, or above T_c . $\gamma_\mu = 2\pi \times 135.5$ MHz/T is the gyromagnetic ratio of the muon.

Zero field μ SR measurements focused on the Up-Down detector pair where coherent oscillations were observed. The data were fitted by

$$A_{\text{ZF}} = A_{\text{rel}} \exp(-\lambda_{\text{rel}} t) + A_{\text{osc}} [(1 - f_{\text{B2}}) \exp(-\Lambda_{\text{B1}} t) \cos(\gamma_\mu B_1 t + \phi_{\text{B1}}) + f_{\text{B2}} \exp(-\Lambda_{\text{B2}} t) \cos(\gamma_\mu B_2 t + \phi_{\text{B2}})], \quad (2)$$

where each component has the meaning described in the main text. Some components were set to zero in different regimes. The total asymmetry, $A_{\text{tot}} = A_{\text{rel}} + A_{\text{osc}}$, was fixed based on the wTF measurements at high T , and allowed to reduce at low T as components became too fast to be resolved. The two phases were globally refined when these components were present, finding abnormal values of $\phi_{\text{B1}} = -53.0(4)^\circ$ and $\phi_{\text{B2}} = -73(2)^\circ$, suggesting complex magnetism. Similarly, $f_{\text{B2}} = 0.381(9)$ was also globally refined when this component was present. All data were fitted using `musrfit` [21].

Muon site calculations were performed using the MuFinder application [22], which ran density functional theory calculations using the CASTEP code [23]. The generalised gradient approximation for solids (PBEsol) [24] was used in all calculations, and a Hubbard U [25] of 4 eV was applied to the Mn d orbitals. A $3 \times 3 \times 2$ supercell was used to ensure that the muons (modelled as rescaled H-atoms) do not self-interact. The lattice parameter was fixed to the value found from geometry optimisation of the pristine cell, where we observed that spin-polarised calculations were essential to reproduce physically-realistic behaviour; spin-polarised calculations were therefore used in all muon-site calculations. Calculations were converged to better than 2 meV/atom using a plane-wave cutoff of 800 eV and a $2 \times 2 \times 2$ k -point grid [26]. The atomic positions were subsequently allowed to relax until the energy and atomic positions have converged to better than 2×10^{-5} meV/atom and 1×10^{-3} Å respectively, and the maximum force on any atom is less than 5×10^{-2} eV/Å. Dipole field calculations were performed using the `muesr` code [27]. The crystal structure was visualized with VESTA [28].

-
- [1] L. Šmejkal, J. Sinova, and T. Jungwirth, Beyond conventional ferromagnetism and antiferromagnetism: A phase with nonrelativistic spin and crystal rotation symmetry, *Physical Review X* **12**, 031042 (2022).
 [2] L. Šmejkal, J. Sinova, and T. Jungwirth, Emerging research landscape of altermagnetism, *Physical Review X* **12**, 040501 (2022).

- [3] L. Bai, W. Feng, S. Liu, L. Šmejkal, Y. Mokrousov, and Y. Yao, Altermagnetism: Exploring new frontiers in magnetism and spintronics, *Advanced Functional Materials* **34**, 2409327 (2024).
 [4] N. Kunitomi, Y. Hamaguchi, and S. Anzai, Neutron diffraction study on manganese telluride, *Journal de Physique* **25**, 568 (1964).

- [5] W. Szuszkiewicz, B. Hennion, B. Witkowska, E. Lusakowska, and A. Mycielski, Neutron scattering study of structural and magnetic properties of hexagonal MnTe, *Physica Status Solidi (c)* **2**, 1141 (2005).
- [6] D. Kriegner, H. Reichlova, J. Grenzer, W. Schmidt, E. Ressouche, J. Godinho, T. Wagner, S. Martin, A. Shick, V. Volobuev, *et al.*, Magnetic anisotropy in antiferromagnetic hexagonal MnTe, *Physical Review B* **96**, 214418 (2017).
- [7] R. Gonzalez Betancourt, J. Zubáč, R. Gonzalez-Hernandez, K. Geishendorf, Z. Šobán, G. Springholz, K. Olejník, L. Šmejkal, J. Sinova, T. Jungwirth, *et al.*, Spontaneous anomalous hall effect arising from an unconventional compensated magnetic phase in a semiconductor, *Physical Review Letters* **130**, 036702 (2023).
- [8] J. Krempaský, L. Šmejkal, S. D'souza, M. Hajlaoui, G. Springholz, K. Uhlířová, F. Alarab, P. Constantinou, V. Strocov, D. Usanov, *et al.*, Altermagnetic lifting of kramers spin degeneracy, *Nature* **626**, 517 (2024).
- [9] D. Kriegner, K. Výborný, K. Olejník, H. Reichlová, V. Novák, X. Marti, J. Gazquez, V. Saidl, P. Němec, V. Volobuev, *et al.*, Multiple-stable anisotropic magnetoresistance memory in antiferromagnetic MnTe, *Nature Communications* **7**, 11623 (2016).
- [10] O. Amin, A. Dal Din, E. Golias, Y. Niu, A. Zakharov, S. Fromage, C. Fields, S. Heywood, R. Cousins, F. Maccherozzi, *et al.*, Nanoscale imaging and control of altermagnetism in MnTe, *Nature* **636**, 348 (2024).
- [11] J. Graham, T. Hicken, R. Regmi, M. Janoschek, I. Mazin, H. Luetkens, N. Ghimire, and Z. Guguchia, Local probe evidence supporting altermagnetism in $\text{Co}_{1/4}\text{NbSe}_2$, preprint arXiv:2503.09193, [10.48550/arXiv.2503.09193](https://arxiv.org/abs/2503.09193) (2025).
- [12] S. Blundell and T. Lancaster, Dft+ μ : Density functional theory for muon site determination, *Applied Physics Reviews* **10**, [10.1063/5.0149080](https://doi.org/10.1063/5.0149080) (2023).
- [13] K. Kluczyk, K. Gas, M. Grzybowski, P. Skupiński, M. Borysiewicz, T. Faş, J. Suffczyński, J. Domagala, K. Grasa, A. Mycielski, *et al.*, Coexistence of anomalous hall effect and weak magnetization in a nominally collinear antiferromagnet MnTe, *Physical Review B* **110**, 155201 (2024).
- [14] A. Hariki, A. Dal Din, O. Amin, T. Yamaguchi, A. Badura, D. Kriegner, K. Edmonds, R. Champion, P. Wadley, D. Backes, *et al.*, X-ray magnetic circular dichroism in altermagnetic α -MnTe, *Physical Review Letters* **132**, 176701 (2024).
- [15] R. D. Gonzalez Betancourt, J. Zubáč, K. Geishendorf, P. Ritzinger, B. Růžicková, T. Kotte, J. Železný, K. Olejník, G. Springholz, B. Büchner, A. Thomas, K. Výborný, T. Jungwirth, H. Reichlová, and D. Kriegner, Anisotropic magnetoresistance in altermagnetic MnTe, *npj Spintronics* **2**, 45 (2024).
- [16] J.-E. Lee, Y. Zhong, Q. Li, M. T. Edmonds, Z.-X. Shen, C. Hwang, and S.-K. Mo, Dichotomous temperature response in the electronic structure of epitaxially grown altermagnet MnTe, *Nano Letters* **25**, 8969 (2025).
- [17] S. Lee, S. Lee, S. Jung, J. Jung, D. Kim, Y. Lee, B. Seok, J. Kim, B. G. Park, L. Šmejkal, *et al.*, Broken kramers degeneracy in altermagnetic MnTe, *Physical Review Letters* **132**, 036702 (2024).
- [18] L. Binci, N. Marzari, and I. Timrov, Magnons from time-dependent density-functional perturbation theory and nonempirical hubbard functionals, *npj Computational Materials* **11**, 100 (2025).
- [19] E. D. Chernov and A. V. Lukoyanov, Electronic correlations in altermagnet mnTe in hexagonal crystal structure, *Materials* **18**, 2637 (2025).
- [20] A. Amato, H. Luetkens, K. Sedlak, A. Stoykov, R. Scheuermann, M. Elender, A. Raselli, and D. Graf, The new versatile general purpose surface-muon instrument (GPS) based on silicon photomultipliers for μ SR measurements on a continuous-wave beam, *Review of Scientific Instruments* **88**, [10.1063/1.4986045](https://doi.org/10.1063/1.4986045) (2017).
- [21] A. Suter and B. Wojek, Musrfit: a free platform-independent framework for μ SR data analysis, *Physics Procedia* **30**, 69 (2012).
- [22] B. M. Huddart, A. Hernández-Melián, T. J. Hicken, M. Gomišek, Z. Hawkhead, S. Clark, F. Pratt, and T. Lancaster, Mufinder: A program to determine and analyse muon stopping sites, *Computer Physics Communications* **280**, 108488 (2022).
- [23] S. J. Clark, M. D. Segall, C. J. Pickard, P. J. Hasnip, M. I. Probert, K. Refson, and M. C. Payne, First principles methods using CASTEP, *Zeitschrift für kristallographie-crystalline materials* **220**, 567 (2005).
- [24] J. P. Perdew, A. Ruzsinszky, G. I. Csonka, O. A. Vydrov, G. E. Scuseria, L. A. Constantin, X. Zhou, and K. Burke, Restoring the density-gradient expansion for exchange in solids and surfaces, *Physical Review Letters* **100**, 136406 (2008).
- [25] B. Himmetoglu, A. Floris, S. De Gironcoli, and M. Cococcioni, Hubbard-corrected DFT energy functionals: The LDA+U description of correlated systems, *International Journal of Quantum Chemistry* **114**, 14 (2014).
- [26] H. J. Monkhorst and J. D. Pack, Special points for brillouin-zone integrations, *Physical Review B* **13**, 5188 (1976).
- [27] P. Bonfà, I. J. Onuorah, and R. De Renzi, Introduction and a quick look at MUESR, the Magnetic structure and mUon Embedding Site Refinement suite, in *Proceedings of the 14th International Conference on Muon Spin Rotation, Relaxation and Resonance (μ SR2017)* (2018) p. 011052.
- [28] K. Momma and F. Izumi, VESTA 3 for three-dimensional visualization of crystal, volumetric and morphology data, *Journal of Applied Crystallography* **44**, 1272 (2011).